Molecular Crystals and Liquid Crystals
Publication details, including instructions for authors and subscription information:
http://www.tandfonline.com/loi/gmcl16

Shape Fluctuations of Red Blood Cells

Mark A. Peterson [a]
[a] Mount Holyoke College, South Hadley, MA, 01875, USA

Version of record first published: 17 Oct 2011.

To cite this article: Mark A. Peterson (1985): Shape Fluctuations of Red Blood Cells, Molecular Crystals and Liquid Crystals, 127:1, 159-186

To link to this article: http://dx.doi.org/10.1080/00268948508080838

Mol. Cryst. Liq. Cryst., 1985, Vol. 127, pp. 159–186
0026-8941/85/1274–0159/$25.00/0

Printed in the United States of America

Shape Fluctuations of Red Blood Cells†

MARK A. PETERSON

Mount Holyoke College, South Hadley, MA 01875 USA

(*Received July 19, 1984*)

The hydrodynamics of shape fluctuations of red blood cells is solved in a model that treats the geometry of the equilibrium shape exactly. The membrane is assumed to be a viscoelastic solid. The consequences for quasi-elastic light scattering are derived, including translational, rotational, and shape fluctuation effects. A light scattering experiment is described which appears to show discrete hydrodynamic modes of the sort predicted by the theory. A detailed comparison shows that the observed amplitudes of the hydrodynamic modes are not correctly given by the viscoelastic solid model. An alternative model is postulated, in which there would be two kinds of hydrodynamic shape fluctuations, corresponding to the two components of the composite membrane, the lipid and the cytoskeleton, moving in some sense independently but constraining each other.

INTRODUCTION

The erythrocyte flicker phenomenon—a kind of shimmering of the red blood cell image in the microscope—was noticed in the last century. While a number of explanations for the phenomenon have been proposed, it was shown quite convincingly by Lennon and Brochard[1] that the effect is a consequence of Brownian shape fluctuations of the cells. They were also the first to attempt a quantitative theory of the effect.

The essential feature of their model is that deformation of the cells increases the bending free energy of the cell membrane, while relaxation of a deformation dissipates energy in the bulk cytoplasm. Thus the two main parameters of the theory are k_c, the bending modulus

†Paper presented at the 10th International Liquid Crystal Conference, York, 15–21st July 1984.

of the membrane, and η, the viscosity of the cytoplasm. They interpreted photomicrographic observations of erythrocyte flicker as a measure of k_c/η, and taking $\eta = 6$ cP, found $k_c = 1.3\text{–}3 \times 10^{-3}$ ergs.

The most drastic simplification in the model of Lennon and Brochard is in the geometry of the cell, which they took to be two infinite, plane parallel membranes separated by a cytoplasmic region with thickness 1–2 microns (whereas, red blood cells are actually disks with radius about 4 microns). The shape fluctuations undoubtedly take place at constant cell volume and surface area, in view of the comparatively large energies necessary to compress the cytoplasm or stretch the membrane. The hydrodynamic modes form a discrete series, instead of a continuum, as they do for an infinite plane model. The rather complicated equilibrium shape of the red blood cell is the arena in which these shape fluctuations take place, and may influence the nature of the fluctuations in ways that are difficult to anticipate. All these complications were (for good reason) omitted in the model of Lennon and Brochard. Still, it is possible to observe the shape fluctuations of red blood cells in detail. Thus it seems worthwhile to carry out the theoretical analysis in detail. That analysis is carried out for realistic red blood cell shapes in this paper for the first time.

Methods for this problem have been developed recently by M.A. Peterson.[2,3] Important subproblems which have been solved are:

1. Expansion of the membrane free energy

$$F = \frac{1}{2} k_c \int_M (2H\text{-}c_0)^2 \, dA + \frac{\mu}{2} \int_M S_{ij} S^{ij} \, dA \qquad (1)$$

about its minimum as a quadratic form in deformation parameters, subject to constraints of constant volume and surface area. (Here H is the mean curvature of the membrane, c_0 is a constant tending to bias the mean curvature, μ is the shear modulus, S_{ij} is the shear strain tensor, and the integrals go over the membrane surface.)[2]

2. Solution of the hydrodynamic problem of the shape relaxation of cells in the spherical limit. (In this limit the equilibrium shape is a sphere and the kinematically allowed amplitude of the fluctuations goes to zero, while the relaxation rates of the discrete modes and their relative amplitudes go to well defined limits).[3]

Section I of the present paper is a natural extension of the work mentioned in item (2) above to the case of non-spherical cells.

In Section II of this paper we consider light scattering from these

shape fluctuations. It is shown that the intensity-intensity correlation function is dominated by, and in a sense selects, a small but representative subset of the hydrodynamic modes, namely the ones which are azimuthally symmetric and have even parity. Thus the interpretation of a properly designed light scattering experiment may not need the full complexity of the hydrodynamic analysis of Section I.

Section III describes a light scattering experiment which reveals the discrete hydrodynamic modes. Comparison with the exactly solved model of Section I shows that the red blood cell membrane does not behave like a two-dimensional viscoelastic solid, as is usually assumed.

Section IV proposes a new dynamical model of the membrane, suggesting that it behaves like a composite material in which a two-dimensional fluid (the lipid) and a two-dimensional solid (the cytoskeleton) have *independent* dynamics except to the extent that they mutually constrain each other. This leads to the notion of two kinds of shape fluctuations: the first kind (fluctuations of the cytoskeleton, constrained by the lipid), and the second kind (fluctuations of the lipid constrained by the cytoskeleton). With this interpretation, the elastic constants of the two components as measured in this experiment are in reasonable agreement with what is known from other experiments.

I. HYDRODYNAMICS OF SHAPE FLUCTUATIONS

Assume the free energy of an incompressible membrane M is that given in Eq. (1), i.e., the sum of curvature and shear free energies. Further assume the membrane dissipation function is

$$D = \frac{\eta_M}{2} \int_M \dot{S}_{ij} \dot{S}^{ij} \, dA \tag{2}$$

where η_M is the membrane surface viscosity. These assumptions have become more or less standard.[4] They represent the membrane as a viscoelastic solid. The consequences of Eq. (1) for the equilibrium shape have been studied by several authors.[5,6] but the consequences of Eqs. (1) and (2) for the dynamics of shape fluctuations of nonspherical cells have never been worked out, except in the approximation of Reference 1, because of the geometrical complexity.

There is, however, no problem in principle. The steps one must take are familiar. We list them below, as a sort of outline, and then comment on the practical details in corresponding subsections.

A. Determine the membrane equilibrium shape, by minimizing Eq. (1) at fixed membrane area and volume.

B. Expand the membrane free energy and dissipation functions in a suitable basis of deformation functions.

C. Expand the bulk flow of the adjoining fluid in a suitable basis. Solve the Navier-Stokes equation.

D. Impose boundary conditions at the membrane surface: continuity of velocity and balance of stress. Include a stochastic driving term in the stress.

E. Solve for the linear response of the membrane shape to the stochastic driving stress using Laplace transforms. The poles of the response function give the relaxation rates of the hydrodynamic modes, and the corresponding eigenfunctions are the hydrodynamic modes themselves. (We are anticipating in this verbal description that all the modes are overdamped).

Not only is it clear what to do in principle, but there are no real practical difficulties either. Step (A) has been well studied already. Step (B) requires us to find matrices whose entries are integrals of known functions over the surface found in (A). These integrals are readily done numerically. Step (C) is familiar. Step (D) requires more numerical integrals over the surface, in order to express the boundary values of the basis functions in the bulk flow in terms of the basis functions on the surface. Step (E) is essentially an eigenvalue problem, and is solved numerically.

The sections below describe the choices made in carrying out this program. It is the description of a practical algorithm which solves the hydrodynamic problem exactly, up to round-off and truncation errors. The problem is well-conditioned at every stage, so these errors should be negligible. It should be noted that the spherical limit of this problem, solved analytically in Reference 3, is an excellent guide to the non-spherical case also.

A. Equilibrium shape

We assume that all shear strain has relaxed in the equilibrium configuration, so that the shape is determined by minimizing the curvature free energy alone (first term in Eq. (1)). It has been shown by Helfrich and Deuling,[5] and by Jenkins,[6] that this prescription leads to shapes indistinguishable from the normal red blood cell shape, although it has been emphasized by Helfrich that the normal oblate shape cannot be the absolute minimum unless c_0 is sufficiently negative. On the other hand Zarda, Chien, and Skalak[7] have shown that

the contrary assumption leads, as a rule, to shapes noticeably different from that observed.

Thus we seek an azimuthally symmetric surface of prescribed area and volume which is topologically a sphere and which minimizes the curvature free energy. Choose the symmetry axis as the x-axis and define coordinates in the surface as follows: let s be arclength from the north pole of the surface measured along a geodesic, and let ϕ be the usual azimuthal angle. Then we have the following calculus of variations problem:

$$\begin{aligned} 0 = \delta\int[&\lambda y^2\cos\theta + \kappa y \\ &+ (\theta' - \cos\theta/y - c_0)^2 y \\ &+ b(y' - \sin\theta)]ds \end{aligned} \tag{3}$$

Here λ and κ are Lagrange multipliers, chosen to keep volume and area constant, and $b(s)$ is a Lagrange multiplier to keep the parameter s equal to the arclength. $\theta(s)$ is the angle that the local tangent vector along a line of increasing s makes with the x-axis. (See Figure 1.) The corresponding Euler-Lagrange equations for x, y, θ, and b are to be solved subject to the boundary conditions

$$\begin{aligned} x(0) &= 0 \\ y(0) &= 0 \\ \theta(0) &= \pi/2 \\ \theta'(0) &= p_0 \text{ (a free parameter)} \\ b(0) &= 0 \end{aligned} \tag{4}$$

The parameters λ, κ, and p_0 must be adjusted so that $b = 0$ when $\theta = \pi$ in order that M be smooth at the equator. Thus the problem of finding M is a two point boundary value problem, readily solved numerically.

All computations in this paper were done on the cell pictured in Figure 1. Its parameters are $\lambda = -11.8741$, $\kappa = -11.4440$, $p_0 = -1.35282$, $c_0 = -1.80376$. The dimensionless ratio A^3/V^2, where A is area and V is volume, is 288 for this cell, in the normal range for

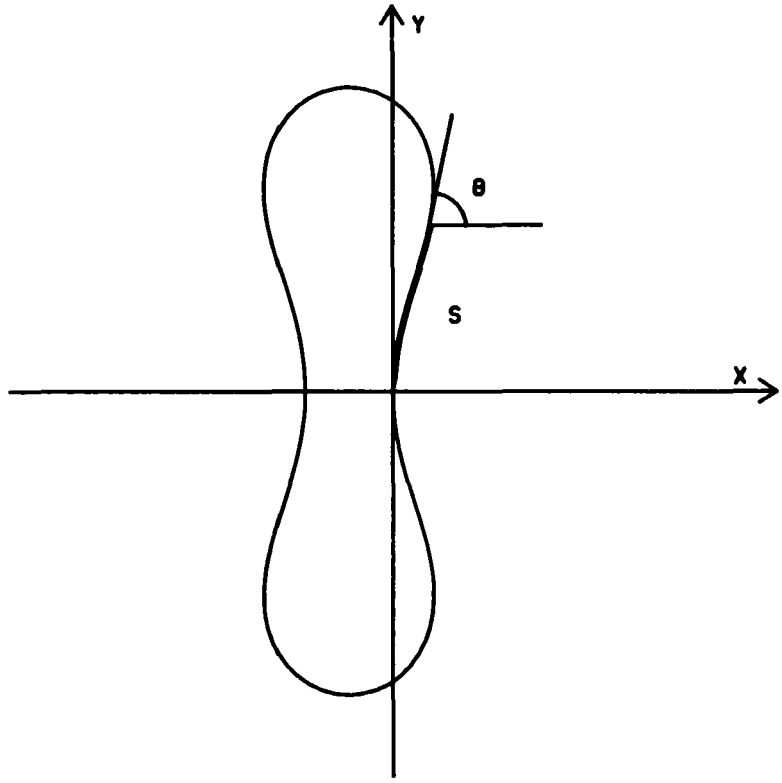

FIGURE 1 A typical solution to Eq. (3) for the red blood cell equilibrium shape. The x-axis is the axis of rotational symmetry. The parameter s is arclength measured from the north pole of the surface, and θ measures the tilt of the local tangent.

human blood cells. The parameters have been scaled so that the equator of the cell is at $s = \pi/2$. The area is then 14.45. Since a normal cell has an area of about 135×10^{-8} cm^2, our unit of length is $a = 3.06 \times 10^{-4}$ cm.

B. Expanding the free energy

Several sets of basis functions are useful for expressing functions on the membrane surface. It is important not to mix them up!

1. Choose the scale of length so that $s = \pi/2$ on the equator. Then the usual spherical harmonics $Y_{lm}(s, \phi)$ are complete, and even orthonormal with respect to the weight function $\sin(s)$. They are not, as a rule, orthonormal with respect to $y(s)$ (which is the area element).

2. The matrix element of the Laplace-Beltrami operator in the basis of spherical harmonics is (up to a sign)

$$(\nabla^2)_{lml'm'} = \int_M \vec{\nabla}\, Y_{lm}^*(s, \phi) \cdot \vec{\nabla} Y_{l'm'}(s, \phi) y(s)\, ds\, d\phi \qquad (5)$$

Since $y(s)$ is a known (tabulated) function, these integrals can be done numerically. The eigenfunctions of the resulting matrix are complete and orthonormal with respect to the area element.

3. An orthonormal basis for normal deformations which conserves volume and area (to first order) can be constructed from the eigenfunctions of the Laplacian. To conserve volume is to be orthogonal to the constant function. Thus we take the constant function (which is, of course, one of the eigenfunctions of the Laplacian) to be the first basis function. To conserve area is to be orthogonal to the mean curvature. Thus we take the mean curvature as the next basis function and apply the Gram-Schmidt procedure to it. Now we apply Gram-Schmidt in turn to the successively higher eigenfunctions of the Laplacian. All basis vectors after the first two are admissible as normal deformations of the membrane. Thus we call this the *admissible* basis. (Of course, by symmetry, the problem breaks up into blocks labeled by parity and by the azimuthal number 'm'. This problem of admissibility occurs only for parity = even, $m = 0$.)

4. One can now find matrix elements of the curvature free energy and the shear free energy (regarded as quadratic forms: see Reference 2) in the admissible basis. This just requires more numerical integrals over the known surface. The eigenvectors of these matrices we will call free energy eigenfunctions. They are complete in the space of admissible normal deformations of the membrane, and orthonormal with respect to the area element.

If one considers the curvature free energy and the shear free energy separately in step 4, one finds quite different behavior. The curvature free energy is uniquely specified by the membrane deformation, and its eigenvalues are well separated (for fixed m). Hence the eigenvector problem is very well posed. The shear free energy, however, is not uniquely specified by the deformation, since tangential motions within the membrane may contribute to shear, but do not change the shape. We assume the shear free energy associated with any shape is the minimum it can be, consistent with that shape and with 2-d imcompressibility. Then it turns out that the shear free energy eigenvalues are all roughly equal (this can also be seen in the spherical limit, Reference 3), so that the eigenvector problem is not so well posed.

For the problem of the total free energy, the result is essentially given by the spherical limit for eigenvalues well above the shear free energy eigenvalue. That is, the free energy eigenfunctions are approximately $Y_{lm}(s, \phi)$ and the eigenvalues are dominated by the curvature term. When the curvature free energy eigenvalues are comparable to, or lower than, the shear free energy eigenvalue, there is much mixing, and the spherical limit is not such a reliable guide.

Since there are many opportunities to make mistakes in a long calculation of this sort, it is important to note that there is a stringent check one can make at this point. There are admissible deformations which are, in fact, not deformations at all, namely rigid translations and rotations. These *must* emerge as free energy eigenfunctions with eigenvalue zero, and in a highly non-trivial way, as these motions will be represented in terms of their local normal and tangential components on the surface. They do in fact appear: the translations as parity = odd, $m = 0, \pm 1$, and the rotations as parity = even, $m = \pm 1$ (the rotation about the symmetry axis is decoupled from shape changes). Thus there can be no doubt of the correctness of the computation to this point.

C. Bulk flow

The analysis here follows Reference 3, which worked out the spherical limit. The shape of the membrane is irrelevant to the bulk dynamics until we consider boundary conditions, so these results are taken over unchanged.

D. Boundary conditions

Let the bulk flow velocities be $\vec{v}^{(\text{int})}$ and $\vec{v}^{(\text{ext})}$, and let the membrane displacement be $\vec{u}$. Furthermore, let the stress tensors for the bulk fluids be $\vec{\vec{\sigma}}^{(\text{int})}$ and $\vec{\vec{\sigma}}^{(\text{ext})}$. Then the boundary conditions are

$$\vec{v}^{(\text{int})}{}_M = \dot{\vec{u}}$$

$$\vec{v}^{(\text{ext})}{}_M = \dot{\vec{u}} \tag{6}$$

$$[\vec{\vec{\sigma}}^{(\text{ext})} - \vec{\vec{\sigma}}^{(\text{int})}] \cdot \hat{n} = -\frac{\delta F}{\delta \vec{u}} - \frac{\delta D}{\delta \dot{\vec{u}}}$$

where $\hat{n}$ is the unit outer normal on the membrane. Expand the bulk quantities in a basis of solutions of the Navier-Stokes equation, and the membrane quantities in a basis of free energy eigenfunctions. The coefficients in these expansions are to be determined by the boundary conditions. Analyze each vector component of these equations by multiplying by $Y_{lm}(s, \phi)$ and integrating over the surface. (There are actually numerical advantages to analyzing the normal components of displacements into free energy eigenfunctions, instead of $Y_{lm}'s$.) By truncation, the boundary conditions become a finite system of linear equations. The coefficients are, as in part (B), numerical integrals of known functions over the surface.

E. Solving the equations

Suppose one wishes to find the first N hydrodynamic modes. One ought to keep $9N$ equations in $9N$ unknowns, since $\vec{v}^{(\text{int})}$, $\vec{v}^{(\text{ext})}$, and $\vec{u}$ each have three components. The problem we have solved is not quite this general, however. In the first place, we have ignored the external fluid. That cuts it down to $6N$ equations. The spherical limit shows that the effect of including the external fluid in the problem is essentially to replace $\eta^{(\text{int})}$ by $\eta^{(\text{int})} + \eta^{(\text{ext})}$. Since $\eta^{(\text{ext})} \ll \eta^{(\text{int})}$ in the blood cell problem, it doesn't seem worth the considerable expansion in the size of the problem to include it. Also we have assumed that the tangential motions of the membrane are determined by the normal motion in such a way as to minimize the shear free energy. This is a constraint, and eliminates the condition of balance of tangential stress. That cuts it down to $4N$ equations.

For azimuthally symmetric modes ($m = 0$) one component of $\vec{v}^{(\text{int})}$ decouples from shape fluctuations and we are down to $3N$ equations. Also, if one analyzes normal deformations into free energy eigenfunctions, N equations can be trivially solved, making the numerical problem that much smaller.

Upon Laplace transformation, $\dot{\vec{u}} \rightarrow -z\vec{u}$. Addition of a Langevin driving term in the pressure makes the linear system inhomogeneous. The poles of the response function are then just at those values of z for which the determinant of the $3N \times 3N$ (or $2N \times 2N$) system of equations vanishes. These are found numerically by stepping z and watching for changes of sign in the determinant. Once again, the spherical limit was a useful guide. In the non-spherical case the hydrodynamic modes are not the same shape as the free energy eigenfunctions, although for the higher modes, if curvature free energy dominates, they are nearly so.

II. LIGHT SCATTERING

The algorithm of the proceeding section solves the standard model of the hydrodynamics of red blood cell shape fluctuations. The solution is not yet in a form that can be compared with experiment, however. Perhaps the simplest method for examining hydrodynamic phenomena on this length and time scale is quasi-elastic light scattering, or photon correlation spectroscopy.[8,9] In this section we work out the consequences of our solution for such an experiment.

The electric field at scattering wavevector $\vec{q}$ is, up to an irrelevant factor,

$$\vec{E}_{\vec{q}}(t) = \int e^{i\vec{q}\cdot\vec{r}}\, \Delta n(t)\, d^3r \tag{7}$$

where Δn is the inhomogeneity in the index of refraction and the integral goes over the scattering volume, which should include many blood cells at random positions, in random orientations, and with random shape fluctuations. Thus $\vec{E}_{\vec{q}}$ should be a Gaussian random variable. At the same time we can anticipate that the phases of the contributions from different cells will be uncorrelated, so that for the purpose of calculating correlation functions we can imagine that Δn refers to a single cell.

The effect of a shape fluctuation is to alter Δn near the surface of the cell. Thus it is natural to split Δn into body and surface terms

$$\Delta n = \Delta n_b + \Delta n_s \tag{8}$$

with a corresponding splitting for the scattered electic field

$$\vec{E}_{\vec{q}} = \vec{E}_b(\vec{q}) + \vec{E}_s(\vec{q}) \tag{9}$$

It is worth noting at this point that Δn_b is even under a parity transformation, by the symmetry of the red blood cell equilibrium shape, but that Δn_s has the parity of the shape fluctuation, which may be either even or odd. Under complex conjugation, therefore,

$$\begin{aligned} \vec{E}_b(\vec{q})^* &= \vec{E}_b(\vec{q}) \\ \vec{E}_s(\vec{q})^* &= \vec{E}_s(\vec{q}) \qquad \text{(even parity)} \\ \vec{E}_s(\vec{q})^* &= -\vec{E}_s(\vec{q}) \qquad \text{(odd parity)} \end{aligned} \tag{10}$$

We must expect that $\vec{E}_b$ will be much larger in magnitude than $\vec{E}_s$. On the other hand, only $\vec{E}_s$ contains information about the shape fluctuations. Fortunately the time scale for shape fluctuations is much shorter than the time scale for translational and rotational diffusion, so that one may hope to separate the contribution of $\vec{E}_s$ experimentally.

If we calculate the intensity-intensity autocorrelation function $c_{II}(t)$, it is clear that the largest terms containing $\vec{E}_s$ will be of a heterodyne form, i.e., they will also contain a product of $\vec{E}_b$'s, so that in a sense we should be seeing heterodyning between the surface and body terms, with the light scattered from the body acting as local oscillator. The present case is different from that usually considered, however,[10] in that the body and surface of the cell move together, so that the local oscillator will be correlated with the surface scattered light, as in homodyne scattering. In short, $c_{II}(t)$ will be a kind of hybrid of homodyne and heterodyne scattering. To be more precise, the relevant terms are

$$c_{II}(t) = \langle \vec{E}_s(t)\vec{E}_b^*(t)\vec{E}_b(0)\vec{E}_s^*(0)\rangle + \langle \vec{E}_s(t)\vec{E}_b^*(t)\vec{E}_s(0)\vec{E}_b^*(0)\rangle + c.c. \quad (11)$$

The second term is the novel one. If E_s and E_b were uncorrelated, it would vanish. In fact, though, it tells us that the odd parity shape fluctuations do not contribute to c_{II}, since in that case, the two terms exactly cancel, by Eq. (10).

Just as the two terms cancel in the odd case, they add in the even case, so that it is enough to consider the first term. Let us assume that translation, rotation, and shape fluctuation are statistically independent processes. Then c_{II} has the form of a product:

$$c_{II} = c^{(\text{shape})}c^{(\text{rot})}c^{(\text{trans})} \quad (12)$$

Furthermore,

$$c^{(\text{trans})} = 1 + e^{-2Dq^2t} \quad (13)$$

where $D = 7 \times 10^{-10}\ \text{cm}^2\text{sec}^{-1}$, the familiar homodyne result. (The value for D is that for an oblate ellipsoid with semiaxes 4,4, and 1 micron, in water at room temperature).[11]

To compute the rotational part, $c^{(\text{rot})}$, choose a coordinate system with the z-axis along the vector $\vec{q}$. If the cell has its symmetry axis

aligned with the vector $\vec{q}$, then we can analyze Δn_b and Δn_s into spherical harmonics:

$$\Delta n_b(\vec{r}) = \sum_L c_L(r)\, Y_{L0}(\psi, \phi) \tag{14}$$

$$\Delta n_s(\vec{r}, t) = \sum_{lm} d_{lm}(r, t)\, Y_{lm}(\psi, \phi) + c.c. \tag{15}$$

As a rule, the cell will not have its symmetry axis aligned with the vector q, but it is a simple matter now to rotate it into any orientation using the Euler angles α, β, and γ, and the familiar representations of the rotation group:[12]

$$\Delta n_b(\alpha, \beta, \gamma) = \sum_{LM} c_L(r)\, Y_{LM}(\psi, \phi)\, D^{(L)}_{M0}(\alpha, \beta, \gamma) \tag{16}$$

$$\Delta n_s(\alpha, \beta, \gamma) = \sum_{lmm'} d_{lm}(r)\, Y_{lm'}(\psi, \phi)\, D^{(l)}_{m'm}(\alpha, \beta, \gamma) \tag{17}$$

Decomposing the plane wave in the usual way

$$e^{i\vec{q}\cdot\vec{r}} = \sqrt{4\pi} \sum_l i^l \sqrt{2l + 1}\, j_l(qr)\, Y_{l0}(\psi, \phi) \tag{18}$$

we can find the scattered fields according to Eqs. (7), (8), and (9)

$$\vec{E}_b = \sqrt{4\pi} \sum_L i^L \sqrt{2L + 1} \int j_L(qr)\, c_L(r)\, r^2 dr\, D^{(L)}_{00}(\alpha, \beta, \gamma)$$

$$\vec{E}_s = \sqrt{4\pi} \sum_{lm} i^l \sqrt{2l + 1} \int j_l(qr)\, d_{lm}(r)\, r^2 dr\, D^{(l)}_{0m}(\alpha, \beta, \gamma) \tag{19}$$

The rotational average now requires us to find

$$\int \langle D^{(l)}_{0m}(\alpha(t), \beta(t), \gamma(t)) D^{(L)}_{00}(\alpha(t), \beta(t), \gamma(t))$$

$$D^{(L')}_{00}(\alpha(0), \beta(0), \gamma(0)) D^{*(l')}_{0m}(\alpha(0), \beta(0), \gamma(0))\rangle\, d\alpha d\beta d\gamma \tag{20}$$

where $\langle\ \rangle$ means average over the values of $\alpha(t)$, $\beta(t)$, $\gamma(t)$ given $\alpha(0)$, $\beta(0)$, $\gamma(0)$, and the integration is with respect to the initial values. In fact, however, rotational diffusion is very slow on the time scale of interest: $D_R = 5 \times 10^{-3}\ \text{sec}^{-1}$ for an oblate ellipsoid with semiaxes

4, 4, and 1 micron in water at room temperature,[13] while the power spectrum of shape fluctuations is known to be in in the range 1–30 Hz.[1] Thus we are justified in setting $t = 0$ in Eq. (20): the cells do not rotate appreciably during a shape fluctuation. We are left with an integral over a product of four spherical harmonics which is easily done, with the result

$$c^{(\text{shape})}c^{(\text{rot})} = 8\pi \sum_{ll'LL'mj} i^{l-L+L'-l'} \langle d_{lm}(q, t)d^*_{l'm}(q, 0)\rangle$$

$$c_L(q)c_{L'}(q)\,(2j+1)\sqrt{(2l+1)(2L+1)(2L'+1)(2l'+1)}$$

$$\begin{pmatrix} L & L' & j \\ 0 & 0 & 0 \end{pmatrix}^2 \begin{pmatrix} l & l' & j \\ m & -m & 0 \end{pmatrix} \begin{pmatrix} ll' & j \\ 00 & 0 \end{pmatrix} \tag{21}$$

where

$$d_{lm}(q, t) = \int d_{lm}(r, t)\, j_l(qr)\, r^2 dr \tag{22}$$

is a kind of Bessel transform, and similarly for $c_L(q)$. Alternatively, we can find $d_{lm}(q, t)$ as

$$d_{lm}(q, t) = \int \Delta n_s\, Y_{lm}{}^*(\psi, \phi)\, j_l(qr)\, d^3r \tag{23}$$

and similarly for $c_L(q)$ (replace Δn_s by Δn_b and Y_{lm} by Y_{L0}).

The last average to do is

$$c^{(\text{shape})}_{ll'm} = \langle d_{lm}(q, t)d^*_{l'm}(q, 0) \tag{24}$$

but since $d_{lm}(q, t)$ is one component of the amplitude of a shape fluctuation (in a rather inconvenient basis), this last expression obeys the hydrodynamics of Section I, and we are formally done.

The factorization of c_{II} given in Eq. (12) is a little schematic. More precisely, it is

$$c_{II}(t) = \sum_{ll'LL'm} c^{(\text{shape})}_{ll'm}(q, t)\, c_L(q)\, c_{L'}(q)\, c^{(\text{rot})}_{ll'LL'm}\, c^{(\text{trans})}(q, t) \tag{25}$$

Here $c^{(\text{rot})}_{ll'LL'm}$ is itself a sum over the index j, as one can read off in Eq. (21). The number of terms in the sum for c_{II} is very large. If each summation index takes only 10 values, we still have 10^6 terms.

There is good reason to believe, though, that the essential result can be obtained with far fewer terms. We note the following facts:

1. There is still approximate rotational symmetry, as shown by the success of the spherical limit in describing the full hydrodynamics. Thus $c^{(\text{shape})}_{ll'm}$ is approximately independent of m. On the other hand $c^{(\text{rot})}_{ll'LL'm}$ depends on m only through a $3 - j$ symbol, which introduces a sign $(-1)^m$ and an otherwise smooth m-dependence. In the sum over m, then, there is approximate cancellation of terms pairwise with one term left over, $m = 0$. (In the spherical limit, this statement is exact).

2. The various amplitudes d_{l0}, c_L, etc., may have either sign and will appear in many respects like random numbers even for a fixed and specified cell geometry. Thus we expect random cancellation *except* in the case $l = l'$ and $L = L'$. All and only such terms are necessarily positive, and of course there is no cancellation among them. These terms should dominate the sum.

3. A computation shows that $c^{(\text{rot})}_{llL0}$ is approximately independent of l and L in the range we will need. In fact it is about equal to 2, and is always between 1 and 3. We will approximate it by a constant.

With these observations $c_{ll}(t)$ becomes very simple. For fixed q, the contribution of the light scattered from the body of the cell, $\Sigma_L|c_L(q)|^2$, is just a multiplicative constant, and can be merged with other constants which we have ignored from the beginning, leaving only

$$c_{ll}(t) = \sum_l \langle d_{l0}(q, t)\, d_{l0}(q, 0)\rangle\, [1 + e^{-2Dq^2t}] \tag{26}$$

It remains only to use hydrodynamics and the equipartition theorem to calculate the first factor.

We found in Section I the orthonormal free energy eigenfunctions $F_a(s, \phi)$ and their corresponding energy eigenvalues E_a ($a = 1, \ldots, 10$), and also the normal displacements of the hydrodynamic modes expressed as linear combinations of the F_a, namely

$$H_A = \sum_a H_{Aa} F_a \tag{27}$$

and their eigenvalues Γ_A (which are the hydrodynamic decay rates). (In the calculations described below we took $A = 1, \ldots, 7$.) By Eq. (23), the coefficient $d_l^{(a)}(q, 0)$ corresponding to the free energy ei-

genfunction F_a is

$$d_l^{(a)}(q, 0) = \delta n \int_M F_a(s, \phi)\, Y_{l0}(\psi(s), \phi)\, j_l(qr(s))\, y(s)\, ds\, d\phi \quad (28)$$

where $\delta n = n_{\text{cell}} - n_{\text{water}}$, and the integral goes over the membrane surface. To find the time-dependence, we must analyze F_a into hydrodynamic modes by inverting Eq. (27) (where we take also $a = 1, \ldots, 7$, so that H_{Aa} is square). Thus

$$\langle d_{l0}(q, t) d_{l0}(q, 0)\rangle = kT(\delta\eta)^2 \sum_{aAb} d^{(a)}{}_{l0}(q)\, [H^{-1}]_{aA}\, e^{-\Gamma_A t}\, H_{Ab}\, d^{(b)}{}_{l0}/E_a \quad (29)$$

Together with Eqs. (26)–(28), this fully specifies $c_{lI}(q, t)$, an experimentally accessible quantity. Although the solution to the model is not quite exact, it is nearly so, and all the essential physics is there. It must be taken as a serious prediction of the standard phenomenological model of the membrane.

$c_{lI}(t)$ is a sum of decaying exponentials, with weights that depend on q and, in a complicated way, on the geometry of the cell and the viscoelastic constants. Ideally one would analyze real data in such a way as to extract all the decay rates and weights, but this is known to be difficult, and to require data of high accuracy. A more generally applicable method of data analysis is to fit a single exponential by some criterion like least squares, accepting that the resulting single decay rate is a weighted average of the actual decay rates.

We have subjected the expression Eq. (26) to such an averaging process for parameter values which cover all plausible possibilities. At one extreme, one might believe the shear modulus is zero, and the membrane is fluid, although one would have to ignore the micropipette aspiration experiments, which seem to measure a shear modulus $\mu \doteq 6 \times 10^{-3}$ dyne/cm.[4] On the basis of experiments which show a buckling of the membrane at a critical pressure, Evans[14] has measured $\mu R^2/k_c \doteq 500$, where R is a length of the order of the radius of the cell. If, on the other hand, one takes k_c from Lennon and Brochard[1] and μ from micropipette experiments,[4] one could obtain $\mu R^2/k_c = 3000$. The surface viscosity could range from 6×10^{-4} surface poise, as inferred from shape recovery experiments, to 4×10^{-6} surface poise, as inferred from diffusion in the membrane.[15]

For various choices of parameters we computed $c_{II}(t)$, sampled it at 32 regular intervals to simulate the data which might accumulate in a 32-channel digital autocorrelator, and then analyzed the result with a least squares program, which was also used in the analysis of real data, to extract the average decay rate. It is clear that the result one obtains in this way may depend on the rate at which $c_{II}(t)$ is sampled. For this reason, the sampling rate was always adjusted to make the total time interval approximately equal to four decay times.

The results are shown in Figure 2. Despite the complexity of the calculations which produced them, they have a simple, common sense meaning. First of all, the rather trivial result for the case $Y \stackrel{def}{=} \mu R^2/k_c = 0$ is a consequence of what is sometimes termed the pathological nature of fluctuations in a fluid membrane. The spherical limit tells us that although there is an interesting spectrum of relaxation rates, going as l^3, the amplitudes of the corresponding exponentials go as l^{-4}. $c_{II}(t)$ is completely dominated by the lowest one and the higher ones would not be seen. The effect of including a shear modulus is to raise the energies of the lowest modes, so that their mean square amplitudes are less pathological. This allows faster modes to be seen, to some extent, but only over a narrow range of

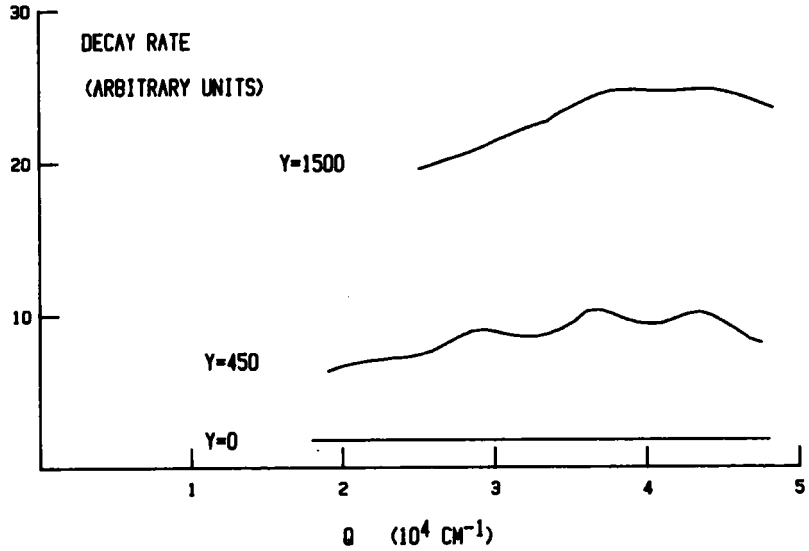

FIGURE 2 Theoretical curves for the decay rate of intensity fluctuations in light scattered from blood cells as a function of q for various viscoelastic membrane model parameters. $Y = \mu a^2/k_c$ is a dimensionless measure of the shear modulus relative to the curvature modulus. $Y = 0$ corresponds to a fluid membrane.

decay rates, corresponding to these modes for which the shear free energy is an appreciable fraction of the total. Yet faster modes, associated with the curvature free energy, still have the very small amplitudes suggested by the spherical limit, and still are not seen. The effect of adding a large surface viscosity is to lower the decay rates by a roughly constant factor and to smooth out the small bumps seen in Figure 2.

Thus the standard phenomenological method of the red blood cell membrane leads to a very definite prediction for a photon correlation experiment. The observed decay rates should have the q-dependence shown in Figure 2. By fitting such a curve one could, if circumstances are favorable, determine the viscoelastic parameters.

We will see in the next section, however, that the experiment gives results inconsistent with the standard model. The membrane cannot be simply a viscoelastic solid.

III. EXPERIMENT

A. Sample preparation

Human blood cells (my own) were drawn into a 10 ml vacutainer containing sodium heparin. The blood was centrifuged, the supernatant drawn off, and the cells resuspended in 0.9% saline solution which had been filtered through a 0.45μ Millipore filter to remove dust particles. This process was repeated three times. After three washings the supernatant appeared clear, an indication that the red cells were intact.

One or two drops of this suspension in 3 ml of filtered saline was the working suspension. It appeared pink and cloudy when it was first made. This suspension was then placed in the sample cell (described below).

The cells were allowed to settle for several hours, by which time most of them had settled to the bottom, forming a bright red layer. Frequently, though not always, some cells remained in suspension and these cells were the subject of the experiment. They are a rather special subset of all the cells, the neutrally buoyant fraction (NBF). Strictly speaking they could not be exactly neutrally buoyant, since they had been centrifuged out with the other cells, but the scale height of their suspension was macroscopic. The presence of the NBF was revealed by the scattered light from a low intensity laser beam. If the NBF was present after a few hours of settling, it seemed to be stable indefinitely. In the microscope it appeared to consist of normal red

blood cells in very dilute suspension. It is not known why the NBF was sometimes absent altogether.

The measurements described below were completed within 12 to 14 hours of drawing the blood. After 24 hours the samples had deteriorated noticeably in the sense that random errors in measured quantities were larger (though within those errors previous results were reproducible). Perhaps the NBF is initially very homogeneous in its properties, and becomes less so as it ages.

B. Experimental layout and procedure

The experimental layout is indicated schematically in Figure 3. Light at 632.8 nm from a 0.5 mW He-Ne laser is focussed into the sample cell. Collection optics on a moveable arm defines the scattering angle and hence q, the scattering wavevector. The scattered light is focussed onto the cathode of a Hamamatsu R464 photon counting photomultiplier. Amplification, discrimination, and pulse shaping are done in the tube base to minimize external noise. The digital pulse train goes to a Langley-Ford autocorrelator. The synthesized autocorrelation function is periodically sent to a TRS-80 microcomputer for analysis and storage on cassette tape, and the autocorrelation restarted. The system was checked and calibrated with a dilute suspension of latex spheres.

A sample of blood cells goes into convection at surprisingly low laser light intensities. When no precautions were taken, this convection was quite obvious as a stable roll pattern in the expanded laser spot on the far wall of the room in which the experiment was done. With the sample in a 1 cm^2 cuvette, convection persisted (although not so obviously) even when the intensity of the beam was made too low to be useful.

Convection could be detected in the measured autocorrelation function, or rather in its residuals after fitting to an exponential function. Systematic motion of the scatterer leads to an autocorrelation function of the form

$$c_{II}(t) = e^{-\Gamma t} \cos \omega t \tag{30}$$

When this is fitted to an exponential function, the residuals near $t = 0$ are large and negative. This behavior of the residuals was a sensitive test for systematic motion. For example, the settling of the cells during sample preparation, in which the systematic velocities were $\leq 10^{-4}$ cm/sec, was obvious.

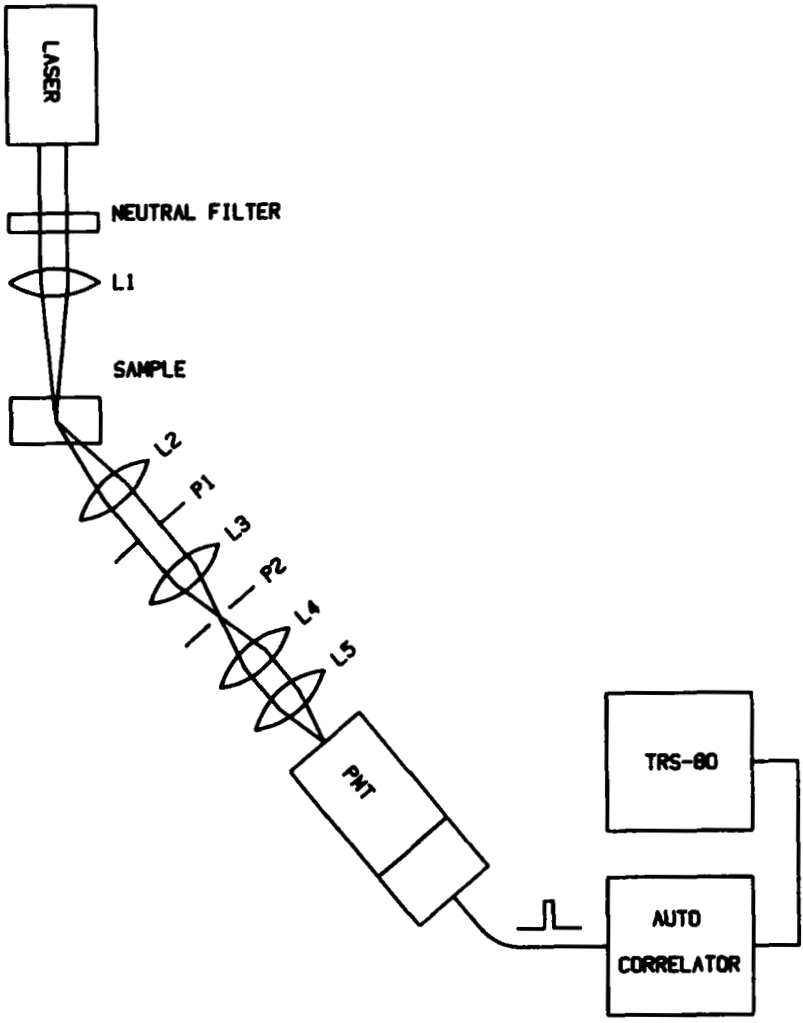

FIGURE 3 Experimental layout for the light scattering experiment described in the text.

Autocorrelation functions taken on a sample in convection were useless as measurements of anything else, as one would expect. They were not reproducible.

In order to suppress convection, the sample cell was made smaller. A ½-inch diameter hole was made through a piece of ⅛-inch lucite. Clean glass microscope cover slips were sealed over both sides with

vaseline, enclosing the sample, and serving as windows into the cell. Even with this arrangement the laser intensity had to be reduced somewhat below 0.5 mW. At a sufficiently low light level, still of usable intensity, the residuals changed character and the autocorrelation function became reproducible over periods of hours. This was interpreted to mean that convection had ceased. The new residuals, characteristic of this experiment, are *positive* near $t = 0$, typical of an autocorrelation function with a mixture of relaxation times, including faster times than that of the best exponential fit. As in the modeling described at the end of Section II, the time per channel was chosen to make the total time over all channels equal to four decay times, as nearly as possible. In fact, though, the measured decay time was not very sensitive to this choice.

Four measurements were made at each angle, each measurement lasting 200 seconds. The latter time was chosen long enough so that the TRS-80 could perform the exponential fit and store the results on tape before the next autocorrelation function was ready. After four measurements, the angle was incremented by 1°. The reported random errors are one standard deviation as determined empirically from the four values obtained at each angle.

C. Experimental results and analysis

Typical results are shown in Figure 4. There are sudden jumps in the observed decay rate as the angle is increased, followed by plateaus where the decay time changes very little. The location of the jumps and the level of the plateaus is more reproducible within a sample than between one sample and another (drawn on different days), as if there were small but significant differences among samples.

This behavior is clearly *not* that predicted by the standard model of the membrane. In the standard model, the decay rate does not change by as much as a factor of two over the whole range, whereas the observed rate changes by more than a factor of five. On the other hand, it is very like what one would see if the fast decay modes, associated with the curvature free energy, were for some reason to have large enough amplitudes to be visible. One seems to see these modes appearing one by one as q is increased, even though the analysis of Section II says this is impossible.

The theoretical analysis leading to the results of Section II is not quite exact. Certain approximations were made. Could any of them be responsible for this failure?

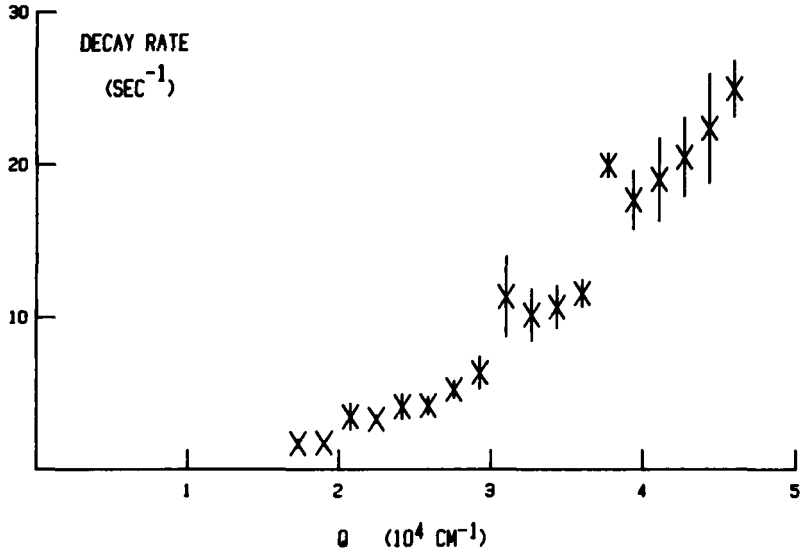

FIGURE 4 Observed decay rate of intensity fluctuations in light scattered from suspended red blood cells.

1. The exterior fluid was neglected, its effect being mainly to change the effective viscosity. Could keeping it somehow favor the visibility of fast, high energy modes? The answer is clearly no.

2. Many terms were left out of the orientational average, on the grounds that they would tend to cancel. Could it be that, for some subtle reason, they *don't* cancel for the fast modes, so that the main contribution to the fast amplitude was missed? Again the answer is no. Such an occurrence could conceivably happen at a special value of q for some mode, but not consistently for all modes and over the entire range.

3. We assumed the tangential motion of the membrane material was constrained by the normal motion, incompressibility, and the minimization of shear free energy. The alternative to this is that stresses from the bulk appreciably excite internal tangential membrane modes. This does not seem to have much to do with shape fluctuations.

To look at the question another way, how much different would the relative amplitudes of the fast hydrodynamic modes have to be for those modes to become visible? The answer is at least an order of magnitude. The analysis of the preceding sections is surely better than that.

The results of Section II are also in accord with common sense. A fast mode must be a high energy mode, but a high energy mode must be a small amplitude mode, by the equipartition theorem. Conversely, a slow mode is a large amplitude mode. The existence of a shear modulus cuts down the amplitudes of the slow modes, but it cannot enhance the amplitudes of the fast modes. As the shear modulus is imagined to increase from zero, it makes the next higher modes visible, but at the same time it tends to bring their decay rates together, so that the measured relaxation spectrum never can show much structure. In words, this is what all our analysis amounts to, and it makes sense. The membrane does not move like a viscoelastic solid.

IV. COMPOSITE DYNAMICS: A NEW MODEL

A. Motivation

It has been accepted for about ten years that the red blood cell membrane is a composite material, consisting of a lipid bilayer and a protein cytoskeleton.[4] This is the picture behind the viscoelastic solid model. In particular, the shear modulus is presumed to be the contribution of the cytoskeleton. Although the light scattering data do not support the viscoelastic solid model, they do suggest a model which is consistent with a composite membrane. Indeed one might call the new model 'composite dynamics,' a phrase which will be defined more precisely in what follows.

It is the equipartition theorem which makes the viscoelastic solid model inconsistent with the light scattering data. In Eq. (29) the mean square amplitude of the mode labeled by 'a' is

$$\langle n_a^2 \rangle = kT/E_a \tag{31}$$

We have tried instead the following alternative prescription:

$$\langle n_a^2 \rangle = kT/(E_a + Z) \tag{32}$$

where Z is a new parameter (i.e., we replace $E_a \to E_a + Z$ in Eq. (29)). The effect is to put an upper limit on $\langle n_a^2 \rangle$ which will drastically alter the amplitude for $E_a \ll Z$ but will not much affect the amplitude for $E_a \gg Z$, as though the system were confined to a box much smaller than the amplitude of the low modes but larger than that of the high

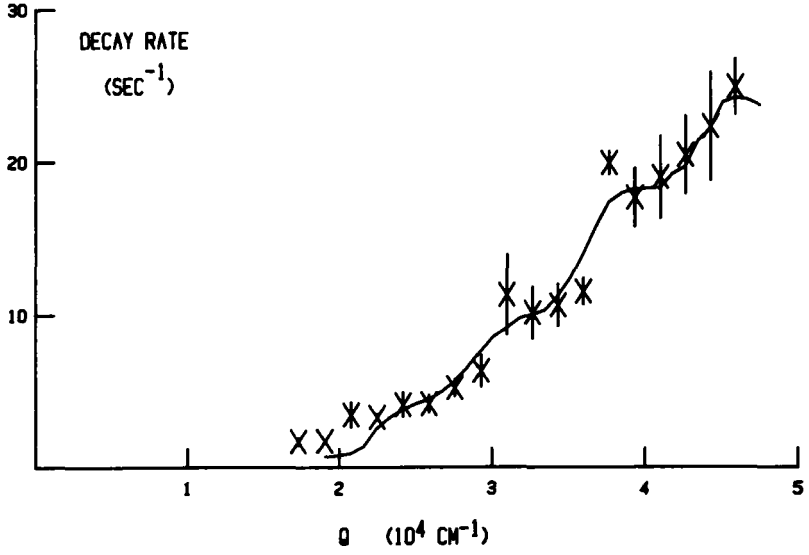

FIGURE 5 A fit to the data of Figure 4 using the amplitude of Eq. (32) instead of Eq. (31), with $k_c = 1.0 \times 10^{-13}$ ergs and $Z = 4 \times 10^{-2}$ erg/cm^2. Here $\mu = 0$ and $\eta_M = 0$.

modes. With such an additional parameter one can obtain quite a good fit to the light scattering data, as shown in Figure 5.

By itself, this is not so interesting, although it is worth repeating that the light scattering data clearly require something of this sort. What is much more interesting is that there is a good physical reason for a parameter Z. This emerges when we ask what its value is. For the fit shown in Figure 5, $k_c = 1.0 \times 10^{-13}$ ergs, $\mu = 0$, $\eta_M = 0$, and $Z = 3.5 \times 10^4 \, k_c/a^2 = 4 \times 10^{-2}$ erg/cm^2. Z has the same units as μ, the shear modulus, *and is of the same order of magnitude as that measured in micropipette experiments,* (from Reference 4, 7×10^{-3} erg/cm^2). This means that the limit on the size of shape fluctuations imposed by Eq. (32) is of the same order of magnitude as the size of the fluctuations of one shear mode of a solid cytoskeleton. One can also put it in terms of shear strain, instead of fluctuation amplitude, since these are proportional, with essentially the same constant of proportionality in every mode: Eq. (32) says one can change the shape freely so long as the shear strain never exceeds a certain fixed amount in any mode, but more shear strain in any mode is not allowed. This way of saying it suggests a "loose cytoskeleton," which can take up a certain amount of shear strain in each mode without any work being done. The numerical closeness of Z and μ

noted above, however, suggests something else: The looseness of the cytoskeleton is due to its thermal excitation. One need not do any work to strain it by an amount which would require the work kT because such strains are already naturally present! To strain it by more, however, one would have to do work.

In short, the observed light scattering data are just what one would expect from a fluid membrane moving freely, but constrained by a 2-*d* solid membrane. This suggests what I call composite dynamics: the two elements of the composite membrane, the lipid and the cytoskeleton, have independent dynamics, but each dynamics takes place within constraints imposed by the other.

B. Discussion

One consequence of this idea is that the light scattering data of Section III correspond to a new phenomenon, and are not the shape fluctuations observed by Lennon and Brochard and others. I call them "shape fluctuations of the second kind." One can picture them as long wavelength undulations of a fluid lipid membrane having very small amplitude, not much larger than the membrane's own thickness, and constrained by the solid framework with which the lipid is in contact.

Meanwhile the solid framework, the cytoskeleton, undergoes its own dynamics, constrained by the lipid. These are shape fluctuations of the first kind, just what has been understood up to now as shape fluctuations pure and simple. The dynamics of the solid is the superposition of all the shear modes. Each shear mode has very small amplitude—indeed, this is what constrains the shape fluctuations of the second kind. But if the solid cytoskeleton has negligible curvature modulus, then each shear mode has about *the same* mean square amplitude, and their superposition could be arbitrarily large. Indeed the amplitude of the shape fluctuations of the first kind is known to be very large, as large as allowed by the constraint of a fluid membrane with a curvature modulus of about the size we measure. Thus one sees a beautiful consistency in shape fluctuations of the first and second kind.

It is ironic that the two components have essentially exchanged their amplitude behavior. The amplitude of the fluid modes are what one should expect of the solid, and the amplitude of the solid modes, at least collectively, are what one should expect of the fluid.

In order for this to work, the fluid must allow much small-scale roughness in the solid. That is, one cannot take seriously the curvature free energy on too small a length scale. This is not at all surprising.

Since we now recognize two kinds of shape fluctuations, we ought to redo the hydrodynamics. Composite dynamics says, though, that the two kinds of shape fluctuation are statistically independent, so that what we call $c^{(\text{shape})}$ is really a product: $c^{(\text{shape}_1)} \times c^{(\text{shape}_2)}$. What we observed was $c^{(\text{shape}_2)}$. Why didn't we see $c^{(\text{shape}_1)}$? That is easy: in this case the analysis of Section II really does apply, and it tells us that $c^{(\text{shape}_1)}$ is essentially structureless! The light scattering method would see only the slowest shape fluctuation of the first kind. The effect is only to add a small, possibly negligible, constant to all the relaxation rates.

The micropipette experiments, Lennon and Brochard, and this experiment are all consistent with the same general picture: a cytoskeleton characterized by a shear modulus $\mu = 7 \times 10^{-3}$ ergs/cm^2, and a lipid characterized by a curvature modulus $k_c = 1 \times 10^{-13}$ ergs, obeying composite dynamics. The question of whether the cytoskeleton has its own small k_c and the lipid its own small μ have not really been carefully investigated yet. Barring such uncertainties, this experiment gives $k_c = 1.0 \pm 0.1 \times 10^{-13}$ ergs for the lipid.

What is most satisfying in the above picture is that all the experiments are accommodated by it. There has always been an implicit contradiction between the shape fluctuation experiments, which seem to say that the membrane is fluid, and the micropipette experiments, which seem to say that it is solid. This contradiction is resolved by composite dynamics, and the light scattering experiment. We find essentially the same k_c as Reference 1, but, through the parameter Z, we also detect the shear modulus of Reference 4. These two values appear consistent for the first time.

C. Formalism

Our account of composite dynamics so far consists of an experimental motivation together with a rather intuitive picture of what is going on. In this last section we attempt to make the model more precise and formal, so that it can be scrutinized and refined.

The best language for stating the model seems to be path integrals. This does not give perfect clarity, as path integrals introduce a kind of vagueness of their own, but vagueness of a suggestive and tolerable kind, one hopes.

Let us suppose that a dynamical system, characterized by coordinates z, evolves along the path $z(t)$ with a probability density given by

$$P^{(1)}[z(t)] \propto \exp(-W^{(1)}[z(t)]) \tag{33}$$

Here $W^{(1)}$ is a functional of the path, and the constant of proportionality would be the path integral of the right hand side. The most probable path is the one satisfying

$$\frac{\delta W^{(1)}}{\delta z(t)} = 0 \tag{34}$$

The solution should coincide with classical hydrodynamics. If we expand W to second order about the minimum we find the Gaussian noise of fluctuations around classical hydrodynamics, etc.

Now suppose there is a second dynamical system which is also described by the coordinates z. The probability density that it follows the path $z(t)$ is given by Eq. (33) with superscripts (2) instead of (1). If the two dynamical systems are statistically independent, then the joint probability density that they *both* follow the path $z(t)$ is just proportional to the product, and this is also true if we ask for the conditional probability that they both follow the particular path $z(t)$ *given* that they follow the same path. That is,

$$P[z(t)] \propto P^{(1)}[z(t)]\, P^{(2)}[z)(t)] \tag{35}$$

This is an example of what composite dynamics might be. It is a prescription within statistical mechanics. It says that the motions of the separate components of the system are to be considered statistically independent for the purpose of finding average quantities, even while they are constrained to be the same. In terms of ensembles, we might imagine a complete ensemble for component 1, and a complete ensemble for component 2, and a sort of "Cartesian product" ensemble for the total system, out of which we select a very small subensemble, namely just those members of the large ensemble in which the coordinates of component 1 and component 2 coincide. To each member of this "diagonal" ensemble we assign a probability proportional to the product of the probability of the first component in its own ensemble times the probability of the second component in its own ensemble. This would be the composite dynamics ensemble, and one could use it to compute averages.

The hydrodynamics of a system which obeyed this statistical law could be found by solving

$$\frac{\delta P}{\delta z(t)} = 0 \tag{36}$$

for the most probable path. The nature of the solution depends on the statistics of each component individually. There may be one unique hydrodynamics for the composite system with properties which, in a sense, combine properties of the components, like the viscoelastic solid model of the composite membrane. To give a very schematic analogy, if $P^{(1)}$ and $P^{(2)}$ were both Gaussians in one variable, centered on different values, then their product would be a Gaussian centered on some intermediate value. But there is no reason in principle that the hydrodynamics should be unique. There might be two paths which were local maxima of the functional P. One can already see this in functions of one variable: the product of two Lorentzians, centered at different places, can have two maxima. The analogous behavior of Eq. (36) would be two kinds of hydrodynamic behavior, like shape fluctuations of the first and second kinds.

Needless to say, we have not solved this statistical mechanical problem. We would like to propose it, though, as a possible solution to some of the puzzling aspects of the behavior of the red blood cell membrane. We even have some notion of what the two kinds of hydrodynamics would have to look like. Both resemble operationally the hydrodynamic behavior of a 2-d fluid alone. They differ in the way that the solid follows the fluid. The solid can follow the fluid mode-for-mode over short distances (shape fluctuations of the second kind), and it can also follow it in a collective way by superposing many modes to follow approximately a single fluid mode (shape fluctuations of the first kind). Whether there is any validity in this theoretical idea will have to await future work, but something of the sort is strongly suggested by the experimental evidence.

Acknowledgments

The experimental work was supported by a George Mason University Faculty Research Grant, and by the physics department of George Mason University. Vacutainers were donated by American Medical Supply of Fairfax, Virginia. The computations were done on a CDC Cyber at the University of Massachusetts, through a time-sharing agreement with Mount Holyoke College.

References

1. F. Brochard and J. F. Lennon, *J. Physique (Paris)*, **36**, 1035 (1975).
2. M. A. Peterson, "*Geometrical Methods for the Elasticity Theory of Membranes*," accepted, *J. Math. Phys.*

3. M. A. Peterson, "*Shape Dynamics of Nearly Spherical Membrane Bounded Fluid Cells,*" this conference.
4. E. A. Evans and R. Shalak, *Mechanics and Thermodynamics of Biomembranes,* CRC Press, Boca Raton, Florida, 1980.
5. W. Helfrich and H. J. Deuling, *J. Physique (Paris),* **37**, 1335 (1976).
6. J. T. Jenkins, *J. Math. Biol.,* **4**, 149 (1977).
7. P. R. Zarda, S. Chien and R. Skalak, *J. Biomech.,* **10**, 211 (1977).
8. B. Chu, *Laser Light Scattering,* Academic Press, New York, 1974.
9. B. Berne and R. Pecora, *Dynamic Light Scattering,* John Wiley & Sons, (1976).
10. See Ref. (9), p. 42.
11. See Ref. (8), pp. 212–13.
12. A. R. Edmonds, *Angular Momentum in Quantum Mechanics,* Princeton Univ. Press, 1957.
13. See Ref. (8), pp. 219–20.
14. E. A. Evans, *Biophys. J.*, **43**, 27 (1983).
15. See Ref. (4), pp. 207–8.